HIGH-ENERGY ELECTRON-INDUCED DAMAGE PRODUCTION AT ROOM TEMPERATURE IN ALUMINUM-DOPED SILICON

J. W. Corbett, L.-J. Cheng*, A. Jaworowski, J. P. Karins, Y. H. Lee†, L. Lindström‡, P. M. Mooney§, G. Oehrlein, and K. L. Wang‖

Institute for the Study of Defects in Solids
Department of Physics
State University of New York at Albany

ABSTRACT

DLTS and EPR measurements are reported on aluminum-doped silicon that has been irradiated at room temperature with high-energy electrons. Comparisons are made to comparable experiments on boron-doped silicon. Many of the same defects observed in boron-doped silicon are also observed in aluminum-doped silicon, but we have observed several not observed, including the aluminum interstitial and aluminum-associated defects. Damage production modeling, including the dependence on aluminum concentration, will be presented.

INTRODUCTION

The radiation-induced defects in silicon responsible for the deterioration of solar cells are mainly impurity-associated defects such as the vacancy-oxygen-carbon complex (the K-center) (ref. 1). One way to improve the radiation tolerance of silicon cells is to remove the undesired impurities, especially oxygen and carbon from the starting material and to prevent their introduction during the cell fabrication processes. Alternatively, a way to reduce the importance of such impurities is to introduce sinks which would act as recombination centers for vacancies and self-interstitials to reduce the chance of the primary defects interacting with the impurities, or perhaps, to introduce an impurity which would trap a vacancy or self-interstitial to form

---

*Present address: Jet Propulsion Laboratory, Pasadena, CA 91103, USA
†Present address: IBM-Thomas J. Watson Research Center, Yorktown Heights, New York 10598, USA
‡Permanent address: Försvaret Forskningsanstalt, S-140 50 Stockholm 80, Sweden
§Permanent address: Department of Physics & Astronomy, Vassar College, Poughkeepsie, New York, 12601 USA
‖General Electric Corporate Research & Development Center, Schenectady, New York 12301, USA

an electronically inactive complex which would not then reduce the minority carrier lifetime in the device. So that we may produce such radiation resistant silicon it is important to understand the damage production mechanisms and defect interactions in electron irradiated silicon. Sutdies which lead to defect characterization and identification and an understanding of defect interactions, particularly of interstitial defects, are in progress. This paper describes some preliminary results of our work in aluminum-doped silicon. This material is interesting because unlike the boron interstitial which is mobile at room temperature, the aluminum interstitial is not mobile at room temperature, and hence, its role in damage production should be different.

EXPERIMENTAL RESULTS

Both EPR and DLTS measurements have been made on electron irradiated aluminum-doped silicon to characterize and identify the defects produced. In all samples oxygen and carbon impurities were present in concentrations of 10^{16}-$10^{18}cm^{-3}$. Diodes were fabricated from float zone and Czochralski grown silicon of 1 Ωcm and 10 Ωcm resistivity irradiated with 1.0 and 1.5 MeV electrons. Most of the diodes were Schottky barrier diodes in which only majority carrier traps are observed although we did observe the minority carrier traps in diffused diodes made from 1 Ωcm material. Figure 1 shows the DLTS spectrum for a diffused diode. The spectrum shows the divacancy peak (H_2) and the K-center peak (H_4 and H_5) both of which are also present in boron doped silicon. In addition, a peak at $E_v + 0.17$ eV (H_1) is observed and also a minority carrier peak at $E_c - 0.29$ eV (E_1). The peak E_1 occurs at nearly the same energy as a boron defect, tentatively identified as $B_I + O_I$ (ref. 2), but the peak intensity is considerably smaller. This could be an aluminum complex and further study is needed to identify this defect.

Figure 2 shows a DLTS spectrum for 10 Ωcm aluminum-doped silicon, in this case a Schottky barrier diode. Again, we observe H_1 but here the intensity compared to the divacancy peak is much smaller, indicating that the concentration of the trap has decreased as has the aluminum concentration. This data plus the absence of this defect in boron-doped material leads to the conclusion that this is an aluminum associated defect. H_3 is the carbon interstitial which anneals at room temperature to form the carbon-oxygen-vacancy complex as was observed in boron-doped silicon (ref. 2,3).

Figure 3 shows the DLTS spectrum for a 1 Ωcm aluminum-doped Schottky diode showing that the peak labeled H_4 and H_5 is resolved into two peaks if the pulse width is reduced sufficiently. At low fluence we believe only the carbon-oxygen-vacancy complex at $E_v + 0.33$ eV (H_4) is present, but that a defect at $E_v + 0.44$ eV (H_5) appears as the fluence is increased. This is observed as a shift of the apparent energy level of the peak toward higher energy as the fluence is increased. We believe this second defect is also present in boron-doped material where we have measured two different capture cross

sections for this peak. We have not yet identified the defect corresponding to the H_5 peak. This spectrum also shows a defect at E_v + 0.55 eV (H_6) which occurs in many aluminum-doped samples. We did not observe this defect in boron doped samples which suggests that it too is an aluminum associated defect.

Isochronal annealing for 20 minute periods was performed on Schottky barrier diodes to study the annealing behavior of these defects. A new DLTS peak appeared at E_v + 0.48 eV (H_7) which appears after annealing at 100°C, continues to grow after the 145°C anneal and then decreases after the 200°C anneal and is essentially gone after a 250°C anneal. Another additional peak is observed after annealing at 400°C at E_v + 0.22 eV (H_8) which increases after a 445°C anneal after which another very small peak at E_v + 0.20 eV also appears. We are continuing to study these new peaks.

EPR measurements in aluminum-doped silicon show that, in addition to the divacancy (G6) (ref. 4), and the carbon interstitial (G12) (ref. 5) which anneals at room temperature to form the carbon-oxygen-vacancy complex (G15) (ref. 3,6), aluminum interstitials (G18) (ref. 7,8) are observed as well as aluminum-vacancy pairs (G9) (ref. 8). The aluminum interstitial was observed to anneal at 200°C by thermal processes forming an aluminum substitutional-aluminum interstitial pair (G19,G20) and a third spectrum (G21) (ref. 9). The aluminum interstitial anneals by an ionization enhanced process at 100°C (Troxell, Chatterjee, Watkins and Kimerling, to be published).

We have not always observed the Al_I defect in our DLTS samples. Although its energy position in the band gap is E_v + 0.17 eV, the DLTS peak is observed at the apparent energy position of E_v + 0.26 eV because of the strong temperature dependence of the capture cross section (ref. 10). We believe it is buried in our carbon-oxygen-vacancy peak and would be more easily observed in samples with low carbon and oxygen content. Table I lists the defects observed by DLTS measurements in both boron-doped and aluminum-doped electron irradiated silicon.

DEFECT PRODUCTION MODELING

In a previous paper we presented results of a computer model for defect production by electron irradiation in boron doped silicon containing carbon and oxygen as impurities and showed that the presence of a defect recombination center could reduce damage produced at a given fluence (ref. 11). The model used is a simplified one described by means of a system of rate equations for defect interactions. Free mobile single vacancies, free mobile self-interstitial atoms and immobile divacancies are created at constant rates during irradiation. We have calculated defect production in boron-doped silicon of different resistivities assuming no other impurities are present, and also for aluminum-doped silicon with the same assumptions. The primary difference in these two systems is that the boron interstitial,

created by the Watkins replacement mechanism, is mobile at room temperature, whereas the aluminum interstitial, created in the same way, is not.

We assume the following defect reactions in boron-doped silicon:

$$I + V \rightarrow \text{recombination} \tag{1}$$

$$I + B_S \rightarrow B_I \quad \text{(ref. 12)} \tag{2}$$

$$B_I + V \rightarrow B_S \tag{3}$$

$$B_I + B_S \rightarrow B_I + B_S \equiv B_I B_S \tag{4}$$

$$B_I + V_2 \rightarrow V + B_S \tag{5}$$

$$V + B_S \rightarrow VB_S \tag{6}$$

$$I + VB_S \rightarrow B_S \tag{7}$$

$$I + V_2 \rightarrow V \tag{8}$$

$$V + V \rightarrow V_2 \tag{9}$$

where V ≡ single vacancy, I ≡ self-interstitial, B_S ≡ substitutional boron, B_I ≡ interstitial boron, and V_2 ≡ divacancy. We assume similar reactions in the aluminum-doped silicon where $A\ell_S$ ≡ substitutional aluminum and $A\ell_I$ ≡ interstitial aluminum replace B_S and B_I in the equations. We have calculated the damage under different irradiation conditions, one with continuous constant flux and the other with pulsed flux, as in the case of a rotating satellite. Table II lists the rate equations and Table III lists the numerical values of parameters used for the calculations.

We present no definitive results here since we are still testing and improving the program. Preliminary results show that at higher doping levels the damage component due to V and V_2 at a particular fluence decreases, while that due to defects involving the dopant increases as more secondary and tertiary defects are produced. In the boron-doped material the major defects in the more heavily doped material are the vacancy-boron substitutional pair and the boron interstitial-boron substitutional pair, whereas in the aluminum-doped material they are the vacancy-aluminum substitutional pair and the aluminum interstitial. This was expected since the aluminum interstitial is not mobile at room temperature and cannot migrate to an aluminum substitutional site. The calculations show equal amounts of damage in both types of materials however. Figures 4 and 5 show calculations for two different aluminum concentrations. The effect of each of these defects on the minority carrier lifetime in the material is not yet determined.

CONCLUSIONS

It is difficult to compare the computer calculations with experimental results at this point since neither aspect of the research is completed. In addition, our measurements have been made on material with large carbon and oxygen concentrations and indeed the carbon interstitial and the carbon-oxygen-vacancy complex have been the dominant defects observed. The aluminum defects predicted by the computer calculations have been observed in EPR studies and we are continuing to study the as yet unidentified DLTS peaks in aluminum-doped silicon. We are also studying p-type silicon with low carbon and oxygen concentrations and with dopants other than aluminum or boron. These experiments should be useful for comparison with the damage production as modeled by the computer calculations and will also provide information on defect characteristics and identity necessary for the construction of the model. This joint approach to the problem of radiation damage in silicon solar cells should give us the necessary information to produce radiation resistant devices.

REFERENCES

1. Lee, Y. H.; Cheng, L. J.; Mooney, P. M.; and Corbett, J. W. in "Solar Cell High Efficiency and Radiation Damage", NASA Conf. Pub. 2002 (NASA, Wash. DC, 1977) p. 165.

2. Mooney, P. M.; Cheng, L. J.; Süli, M.; Gerson, J. D.; and Corbett, J. W.: Phys. Rev. B 15, 3836 (1977).

3. Lee, Y. H.; Cheng, L. J.; Gerson, J. D.; Mooney, P. M.; and Corbett, J. W.: Solid State Comm. 21, 109 (1977).

4. Watkins, G. D.; and Corbett, J. W.: Phys. Rev. 138A, 543 (1965).

5. Watkins, G. D.; and Brower, K. L.: Phys. Rev. Letters 36, 1329 (1976).

6. Lee, Y. H.: Corbett, J. W.; and Brower, K. L.: Phys. Stat. Sol. (a) 41, 637 (1977).

7. Brower, K. L.: Phys. Rev. B1, 1908 (1970).

8. Watkins, G. D.: Phys. Rev. 155, 802 (1967).

9. Watkins, G. D.: in Radiation Damage in Semiconductors (Dunod, Paris, 1967) p. 97.

10. Troxell, J. R.; and Watkins, G. D.: Bull. Am. Phys. Soc. 23, 214 (1978).

11. Cheng, L. J.; Sours, P. W.; Karins, J. P., Corelli, J. C.; and Corbett, J. W. in "Solar Cell High Efficiency and Radiation Damage", NASA Conf. Publ. 2020 (NASA, Wash. DC, 1977) p. 179.

12. Watkins, G. D.: Phys. Rev. B12, 5824 (1976).

TABLE I.- DEFECTS OBSERVED BY DLTS IN BORON-DOPED AND Aℓ-DOPED ELECTRON IRRADIATED SILICON

	Peak	Energy Level	Capture Cross Section (cm^2)	Annealing Temperature	Identity
B-doped and Aℓ-doped Si	H_2	E_v + 0.23 eV	$\sigma_p = 3 \times 10^{-16}$	out 270°C	$[V_2]^+$
	H_3	E_v + 0.29 eV	$\sigma_p = 3 \times 10^{-16}$	out 30°C	$[C_I]^+$
	H_4	E_v + 0.33 eV	$\sigma_p = 2 \times 10^{-16}$	in 30°C, out 400°C	$[V+O+C]^+$
	H_5	E_v + 0.44 eV	$\sigma_p = 10^{-19}$	out 400°C	?
B-doped only		E_c - 0.27 eV	$\sigma_p = 2 \times 10^{-13}$	out 170°C	$[B_I+O_I]$ (tentative)
		E_v + 0.30 eV	$\sigma_p = 2 \times 10^{-16}$	in 170°C, out 400°C	[B+O+V] (tentative)
Aℓ-doped only	H_1	E_v + 0.17 eV	$\sigma_p = 4 \times 10^{-15}$		Aℓ associated
	H_6	E_v + 0.55 eV	$\sigma_p = 10^{-19}$		?
	H_7	E_v + 0.48 eV		in 145°C, out 250°C	?
	H_8	E_v + 0.22 eV		in at 400°C	?
	H_9	E_v + 0.20 eV		in at 445°C	?
	E_1	E_c - 0.29 eV			?

TABLE II.- RATE EQUATIONS

$$\frac{\partial[V]}{\partial t} = G - 4\pi(D_V+D_I)R_{VI}\,[V][I] - 4\pi D_V[V](2\,R_{VV}[V] + R_{VB_I}[B_I] + R_{VB_S}[B_S]) + 4\pi D_{B_I}[B_I]R_{V_2B_I}[V_2] + 4\pi D_I[I]R_{V_2I}[V_2]$$

$$\frac{\partial[I]}{\partial t} = G + 2G_{V_2} - 4\,(D_V+D_I)R_{VI}[V][I] - 4\,D_I[I]\,(R_{IB_S}[B_S] + R_{IVB_S}[VB_S] + R_{V_2I}[V_2])$$

$$\frac{\partial[V_2]}{\partial t} = G_{V_2} - 4\pi D_{B_I}R_{V_2B_I}[B_I][V_2] - 4\pi D_I R_{V_2I}[I][V_2] + 8\pi D_V R_{VV}[V]^2$$

$$\frac{\partial[B_S]}{\partial t} = -4\pi D_I R_{IB_S}[I][B_S] + 4\pi D_V R_{VB_I}[V][B_I] - 4\pi D_{B_I}R_{B_IB_S}[B_I][B_S] + 4\pi D_{B_I}R_{V_2B_I}[B_I][V_2] - 4\pi D_V R_{VB_S}[V][B_S] + 4\pi D_I R_{IVB_S}[I][VB_S]$$

$$\frac{\partial[B_I]}{\partial t} = 4\pi D_I R_{IB_S}[I][B_S] - 4\pi D_V R_{VB_I}[B_I][V] - 4\pi D_{B_I}R_{B_IB_S}[B_I][B_S] - 4\pi D_{B_I}R_{V_2B_I}[B_I][V_2]$$

$$\frac{\partial[B_IB_S]}{\partial t} = 4\pi D_{B_I}R_{B_IB_S}[B_I][B_S]$$

$$\frac{\partial[VB_S]}{\partial \tau} = 4\pi D_V R_{VB_S}[V][B_S] - 4\pi D_I R_{IVB_S}[I][VB_S]$$

[ ] indicate concentration

TABLE III.- NUMERICAL VALUES OF PARAMETERS USED FOR COMPUTER CALCULATIONS

Capture Radii

$$R_{VI} = R_{VV} = R_{VB_I} = R_{VB_S} = R_{V_2B_S} = R_{V_2I}$$
$$= R_{IB_S} = R_{IVB_S} = R_{B_IB_S} = 5 \text{ Å}$$

Generation rates

$G = 5 \times 10^{12}/cm^2/sec$ generation rate of V,I

$G_{V_2} = 5 \times 10^{9}/cm^2/sec$

Diffusion coefficients

$D_I = 3.16 \times 10^{-3} cm^2/sec$

$D_V = 4.15 \times 10^{-7} cm^2/sec$

$D_{B_I} = 1.00 \times 10^{-6} cm^2/sec$

$D_{A\ell_I} = 0$

Rotating satellite

flux on for 10^{-4}sec $(g, G_{V_2} = 0)$

flux off for 10^{-4}sec $(G, G_{V_2} = 0)$

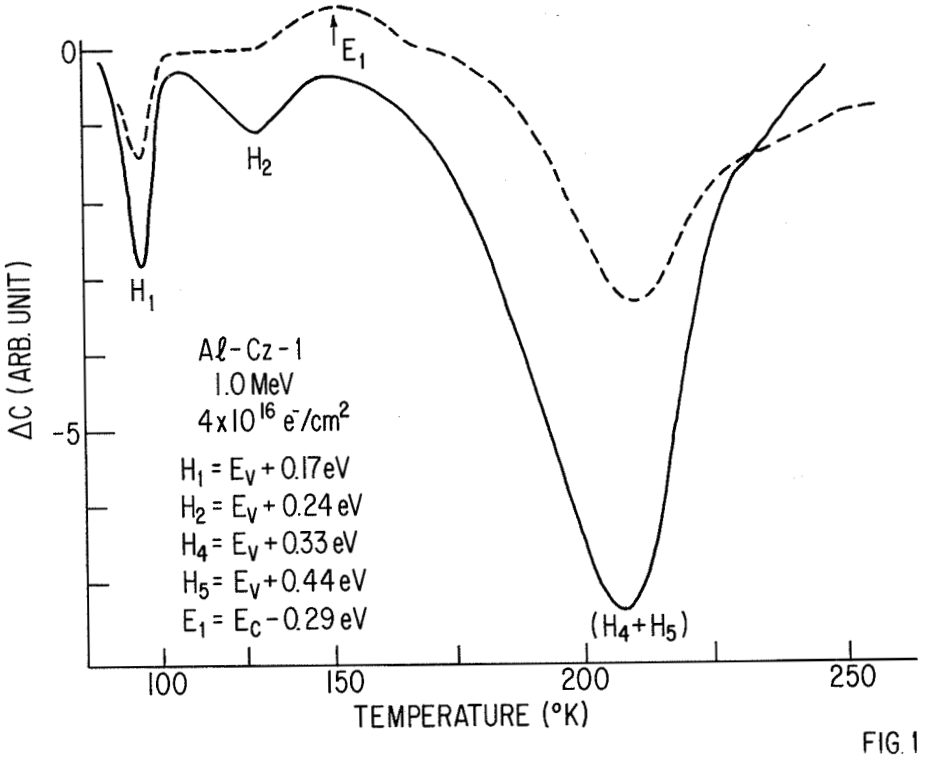
0
-5
ΔC (ARB. UNIT)
E1
H2
H1
Aℓ-Cz-1
1.0 MeV
4x10^16 e⁻/cm²
H1 = EV + 0.17eV
H2 = EV + 0.24 eV
H4 = EV + 0.33 eV
H5 = EV + 0.44 eV
E1 = EC - 0.29 eV
(H4+H5)
100
150
200
250
TEMPERATURE (°K)

FIG. 1

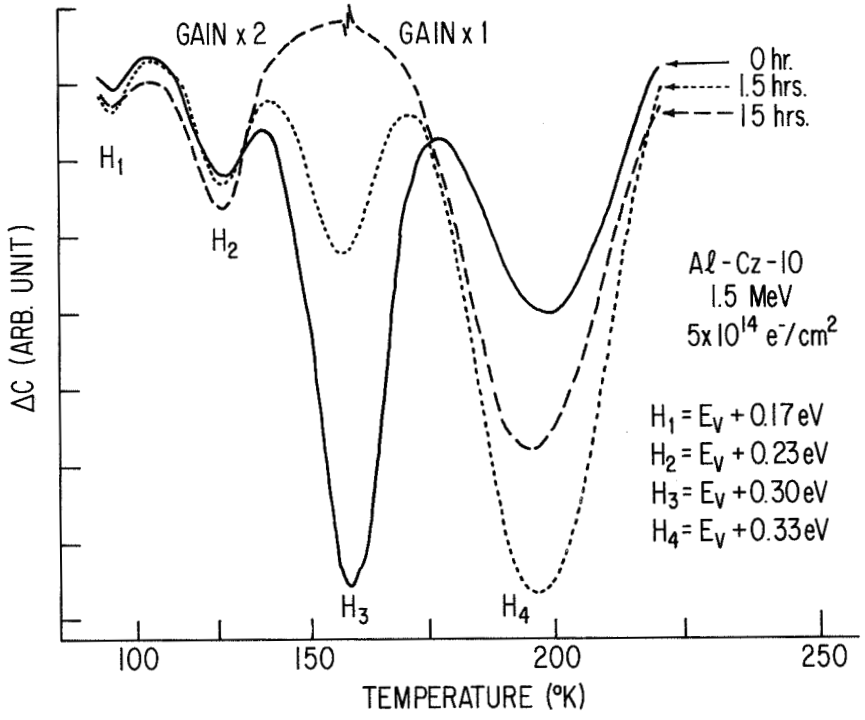
GAIN x 2
GAIN x 1
0 hr.
1.5 hrs.
15 hrs.
H1
H2
H3
H4
ΔC (ARB. UNIT)
Aℓ-Cz-10
1.5 MeV
5x10^14 e⁻/cm²
H1 = EV + 0.17eV
H2 = EV + 0.23eV
H3 = EV + 0.30eV
H4 = EV + 0.33eV
100
150
200
250
TEMPERATURE (°K)

FIG. 2

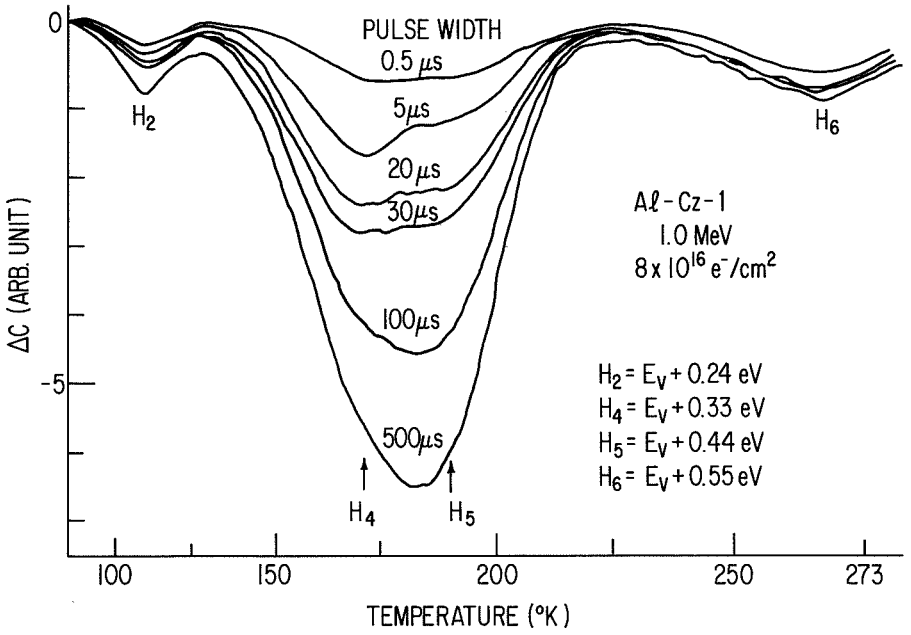
PULSE WIDTH
0.5 μs
5μs
20μs
30μs
100μs
500μs
H2
H4
H5
H6
Aℓ-Cz-1
1.0 MeV
8 x 10^16 e⁻/cm²
H2 = EV + 0.24 eV
H4 = EV + 0.33 eV
H5 = EV + 0.44 eV
H6 = EV + 0.55 eV
ΔC (ARB. UNIT)
0
-5
100
150
200
250
273
TEMPERATURE (°K)

FIG. 3

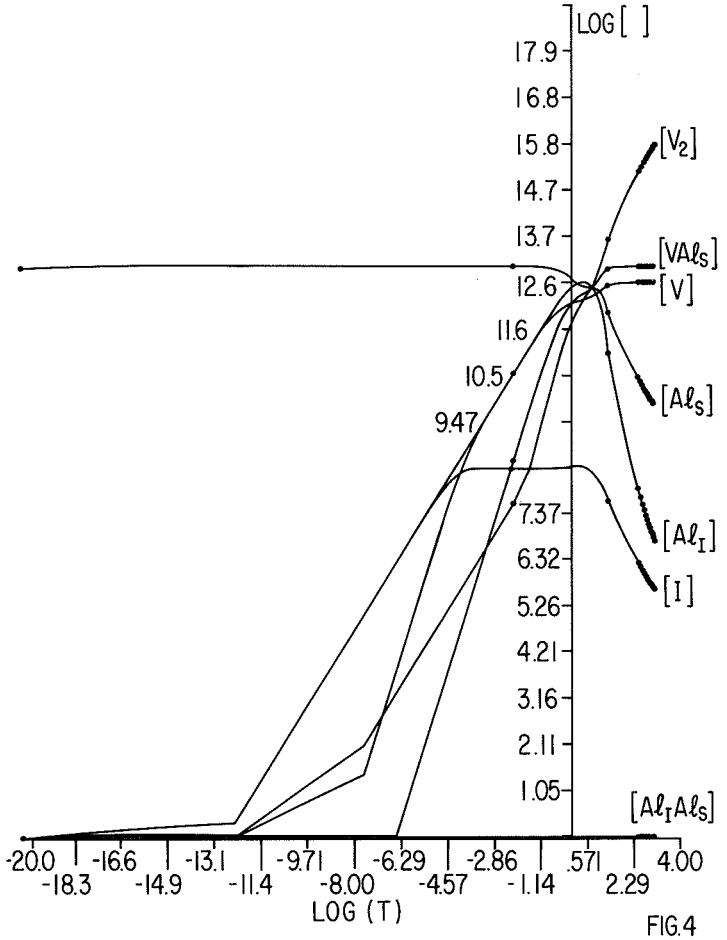
LOG[ ]
17.9
16.8
15.8
14.7
13.7
12.6
11.6
10.5
9.47
7.37
6.32
5.26
4.21
3.16
2.11
1.05
[V2]
[VAℓS]
[V]
[AℓS]
[AℓI]
[I]
[AℓIAℓS]
-20.0
-18.3
-16.6
-14.9
-13.1
-11.4
-9.71
-8.00
-6.29
-4.57
-2.86
-1.14
.571
2.29
4.00
LOG (T)

FIG.4

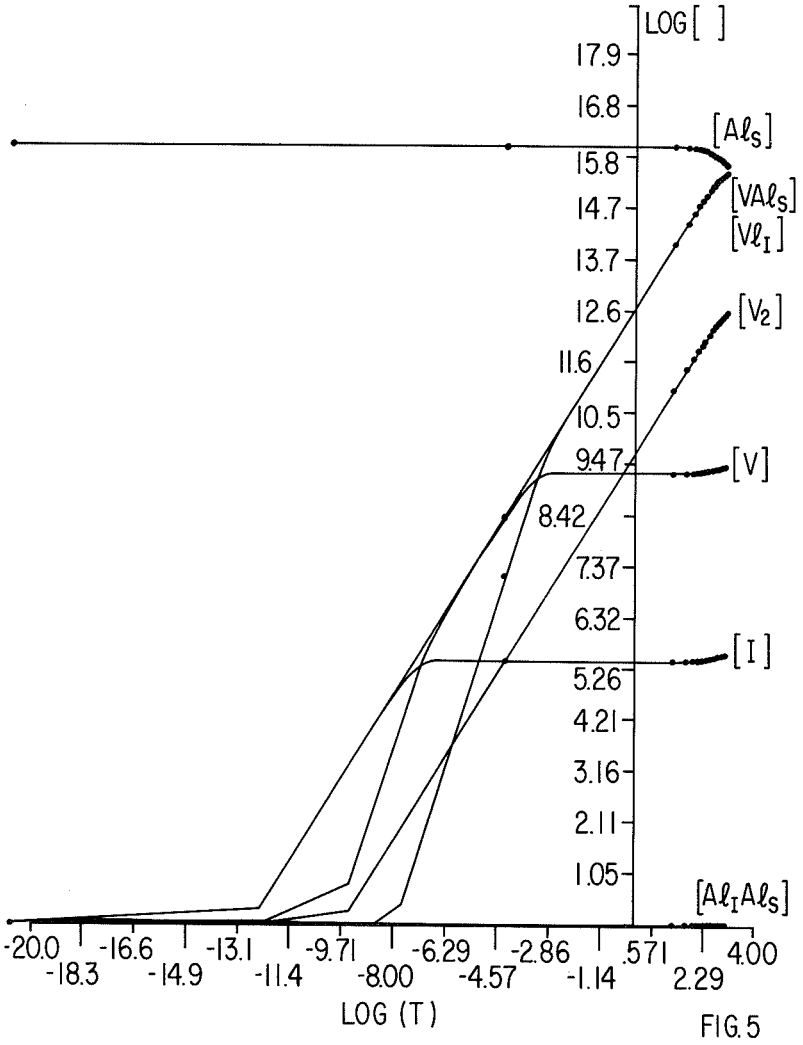
LOG[ ]
17.9
16.8
15.8
14.7
13.7
12.6
11.6
10.5
9.47
8.42
7.37
6.32
5.26
4.21
3.16
2.11
1.05
[Alₛ]
[VAlₛ]
[Vl_I]
[V₂]
[V]
[I]
[Al_IAlₛ]
-20.0
-18.3
-16.6
-14.9
-13.1
-11.4
-9.71
-8.00
-6.29
-4.57
-2.86
-1.14
.571
2.29
4.00
LOG (T)

FIG. 5